Decay of air cavity slamming pressure oscillations during sloshing at high fillings

Bjørn C. Abrahamsen* and Odd M. Faltinsen

Department of Marine Technology &
Centre for Ships and Ocean Structures, CeSOS
Norwegian University of Science and Technology, NTNU
O. Nielsens vei 10, Tyholt N-7491 Trondheim, Norway
bjornchr@ntnu.no, odd.faltinsen@ntnu.no
* Presenting author

The roof inside a ship tank is exposed to different impact load scenarios during sloshing at high fillings. This work is a detailed study of the load exerted near the tank corner when the incoming wave entraps an air pocket. This air pocket is compressed by the wave. After this initial compression the pressure inside the air pocket starts to oscillate qualitatively as a damped mass-spring system. A similar type of impact occurs when a breaking shallow water wave entraps an air pocket on a sea wall. Different sources for the decay mechanism has been proposed such as air leakage. In this work experiments and numerical work using the boundary element method (BEM) is carried out to investigate this decay mechanism in detail.

The tank is shown in figure 1 and is considered in both the experiments and the numerical work. The dimensions of the tank is height H=$0.98[m]$ and breadth L=$1.0[m]$. For the experiments the length in the z-direction is $0.1[m]$. The filling height h=$0.85H$.

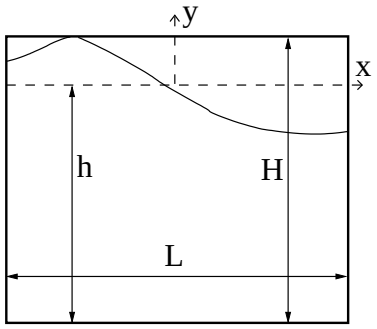

Figure 1: The tank used in the numerical and experimental work.

The surge excitation $\eta(t)$ is constructed so that the air pocket slamming event occurs on the first contact with the roof. It is chosen as $\eta(t)$=$\sum_{i=1}^{n}\eta_i(t)$ where

$$\eta_i(t) = \begin{cases} \eta_{ai}[cos(\sigma_i(t-t_{si}))-1] & t \geq t_{si} \\ 0 & t < t_{si} \end{cases} \quad (1)$$

Each term i in the sum triggers the corresponding natural mode in the tank, because the excitation frequency of each term corresponds to the natural frequency of that mode. Here η_{ai} is the excitation amplitude. t_{si} is the time when the excitation signal i starts. g is the acceleration of gravity. σ_i is the natural frequency of the natural modes.

$$\sigma_i = \sqrt{\frac{g\pi i}{L}\tanh\left(\frac{h\pi i}{L}\right)} \quad (2)$$

For the air pocket named "case 6" reported here, modes 1, 5 and 9 are used. After some time of exciting modes 5 and 9, they appear as superposed standing waves. Then a signal corresponding to the first mode is added. The time instant t_{si} when the different modes starts is tuned so that the wave hits the roof with an air pocket. For "case 6" the following parameters were chosen: t_{s1}=$3.820[s]$, t_{s5}=$0.5652[s]$, t_{s9}=$0.0[s]$, η_{a1}=$0.0202[m]$, η_{a5}=$0.00145[m]$ and η_{a9}=$0.00077[m]$. The experimental excitation system did not exactly reproduce its input signal, so the analytical signal in equation 1 is fitted to the measured position in the experiment and must be considered approximate. For the numerical simulations the measured surge motion and acceleration are used directly as input. The resulting pressure time history inside the air pocket is quite repeatable. The latter is true at least for impact events with not too large impact velocity, i.e. less than approximately $0.4[m/s]$.

A tank made of $20[mm]$ thick acrylic sheets is used for the experiments. Horizontal tank position and acceleration are measured and four pressure sensors are attached to the roof at the air cavity. The pressure sensors measure nearly uni-

form pressure inside the air pocket at a sampling frequency of (9600Hz). The pressure sensor P2 as shown in figure 2 is used in the next plots. This is located $19[mm]$ from the left tank wall. The average pressure time histories for 13 runs are plotted in figure 3 for the air pocket named "case 6". The impact velocity along the left wall and the initial air cavity volume are estimated to be V_0=$0.39[m/s]$ and Ω_0=$9.8 \cdot 10^{-4}[m^2]$, respectively. The initial velocity is measured when the wave peak passes y=$0.14[m]$. The plot contains a 95% confidence interval assuming a normal distribution of the random error. The pressure curve is aligned so that the zero down crossing between the first pressure maximum and the first pressure minimum is occuring at the same time instant in all 13 runs.

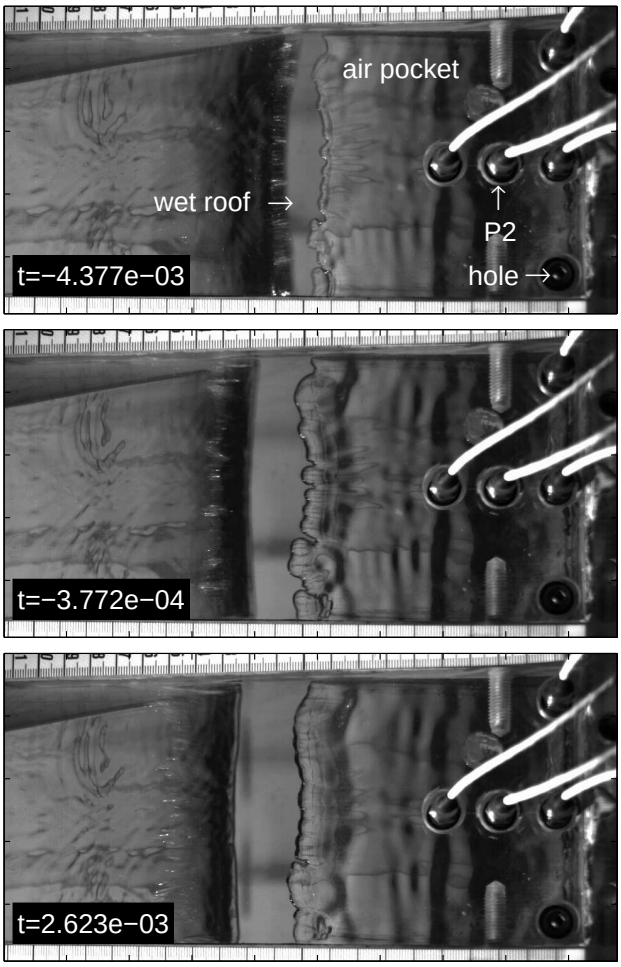

Figure 2: Pictures taken from above the tank at three time instances for case 618. The time is referring to the plot in figure 3. The hole is closed for this run.

From figure 3 we see that a large part of the energy stored in the air pocket is lost during the time from the first pressure maximum to the first pressure minimum. A high speed camera is used extensively from different angles to identify any air leakage or other sources causing this decay. If the system behaved as a mass-spring system we would say that the decay is caused by damping. However, we should realize that the analogy to a mass-spring system is a simplification.

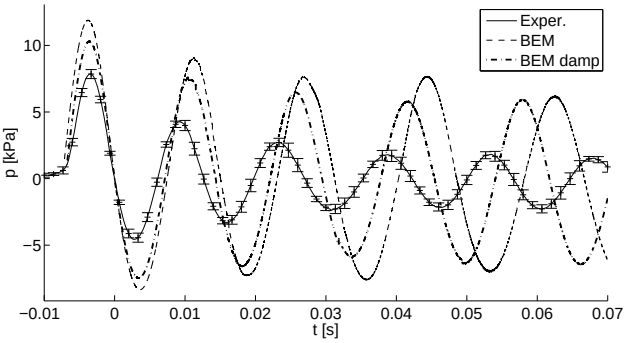

Figure 3: The dynamic pressure time history of pressure inside the air pocket for experiment and BEM. For the experiments the error bars shows the 95% confidence interval.

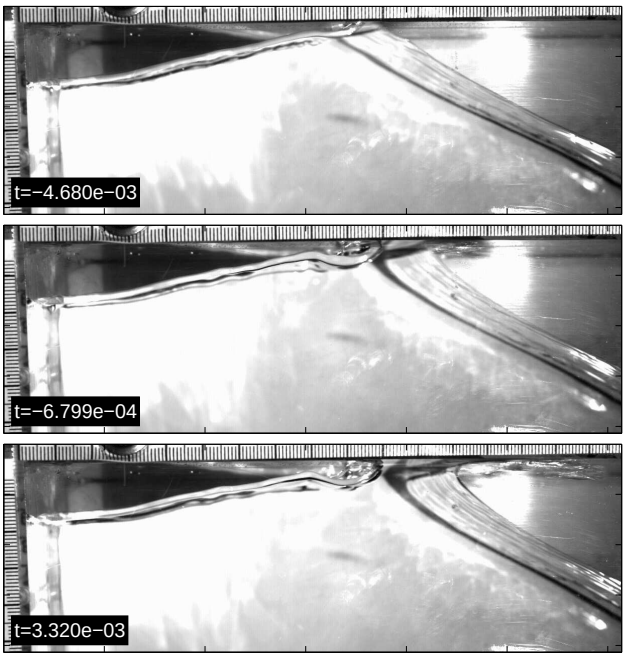

Figure 4: Pictures taken of the upper left corner at three time instances for case 622. The time is referring to the plot in figure 3. The hole is closed for this run.

In the pictures in figure 2, the pocket is seen from above. This is one of the runs for case 6, that is run 618. In figure 4 nearly the same time instances is shown for run 622, where the camera where mounted to see the air pocket from the side. The pressure at the time instants can be found in figure 3. In both figures 2 and 4 the upper images are taken prior to the first pressure maximum. The second images show the pocket when the pressure is nearly zero, while the last images

show the pocket when the pressure is close to the first minimum. These images show that the air pocket is closed in this period. This means that no air leakage is observed and is not likely to be present during the period where significant energy leaves the pocket. There is also not seen any leakage in the time period after these images and until the water exit phase. However, there is air leakage prior to closure in the area where the wave touches the roof initially. This air leakage leads to a pointed wave peak which is important to capture in a numerical model. Before the air pocket closes there are also minor 3D effects caused by capillary waves due to meniscus effects interacting with the gravity waves.

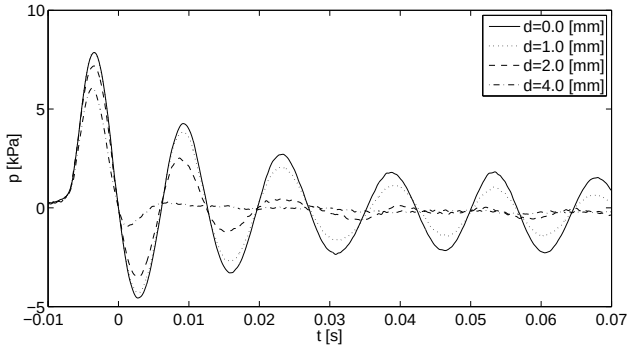

Figure 5: Effect of different hole diameters on the dynamic pressure inside the pocket for pressure cell P2.

To elaborate further on the damping effect of leakage, a hole was made in the tank roof to puncture the air pocket. The location of this hole is shown in figure 2. These were circular holes with diameter d=$0, 1, 2, 4[mm]$. The effect on the pressure time history can be seen in figure 5. Here the zero diameter results are the same curve as in figure 3. The curves for $d > 0$ is the mean of three runs at each diameter. As seen from the figure, the effect of leakage appears as damping, affecting both the peak pressure and the decay of the pressure oscillations. Even quite small holes damp significantly the pressure time history. The effect of these holes as a damping mechanism is consistent with the results from the empirical damping model used by Faltinsen and Timokha [1].

For the mathematical model incompressible potential flow is assumed for the water and for the compressible air pocket the pressure is assumed to be uniform in space with an adiabatic pressure-density relationship. The fully nonlinear boundary conditions are applied at the free surface. This is similar to the model used by Zhang et. al. [2] who investigated a breaking wave towards a sea wall. A simplified 1D stationary incompressible model is used for the air before roof contact. For the numerical discretization a linear boundary element method BEM is used similar to Greco et. al. [3]. For the time integration a 4th order Runge-Kutta method is applied.

Different ways to treat the initial contact between the free surface and the roof exist. One can disregard the air flow and do a Wagner type of impact analysis similar to Greco et. al. [3]. Then the air escaping the pocket area prior to closure is not modelled at all, and the BEM solver is stepped across the roof and then the initial local effect of slamming is accounted for by using Wagner's slamming theory. From the experiments it is clearly seen that there is no jet towards the air pocket, while there is a jet present towards the free surface outside the pocket. A Wagner type of model implies a jet flow in both directions. It is also seen that the air affects the free surface when the distance between the free surface and the roof is less than approximately $3[mm]$. As the air evacuates the pocket prior to closure there is low pressure at the top of the wave due to the high velocity of the escaping air. This low pressure leads to a more pointed free surface compared to the case where there would be no air effect. Since the air flow so strongly affects the free surface in the impact zone, it cannot be neglected, hence the Wagner model is not sufficient for our problem.

To include some of the effect of the air before a closed air cavity occurs a simplified stationary incompressible 1D assumption is made for the air. Mass conservation yields the following expression for the relative horizontal velocity u_a in the air above the incoming wave prior to closure:

$$u_a = \frac{1}{h(x,t)} \int_{-L/2}^{x} \frac{\partial \phi}{\partial n} d\tau \qquad -L/2 < x < L/2 \tag{3}$$

Here $h(x,t)$ is the distance between the free surface and the roof. $\partial\phi/\partial n$ is the velocity component normal to the free surface and τ is an integral variable along the x-axis. A drawback is that the 1D model is singular as the gap $h(x,t)$ becomes zero. Then Bernoulli's equation for the air assuming stationary air flow produces an extra term in the dynamic boundary condition for the

water, which on the free surface is given as:

$$\frac{D\phi}{Dt} = \frac{1}{2}\nabla\phi\cdot\nabla\phi - gy + \frac{1}{2}\left(\frac{d\eta}{dt}\right)^2 - x\frac{d^2\eta}{dt^2} + \frac{\rho_a}{2\rho_w}u_a^2 \quad (4)$$

Here ρ_a, ρ_w is the density in air and water. and D/Dt is the material derivative. The expression is valid along the free surface as the wave approaches the roof and until the wave touches the roof. Damping of the sloshing motion was identified in the experiments. This where investigated by adding a Rayleigh damping term $-\mu\phi$ to the free surface boundary condition during the sloshing phase prior to slamming. The dynamic boundary condition in the sloshing phase is similar to eq. 4 with u_a=0. μ where found by linearizing the free surface boundary condition and fitting it to experimental decay tests. A major physical source of this damping is associated with the viscous boundary layers along the tank walls.

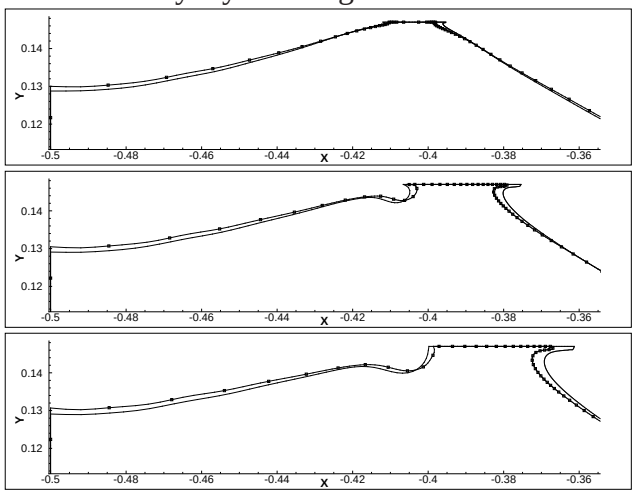

Figure 6: The free surface configuration at the same time instants as in figure 4. The dotted line is the damped BEM results while the line is the undamped results. The dots shows every fifth node point of the BEM.

The pressure time history of the BEM is compared with the experiments in figure 3. The initial volume in the BEM is 1.11e-3 [m^2]. while the initial impact velocity is 0.424 [m/s]. For the Rayleigh damped BEM the initial volume is 1.03e-3 and the initial velocity is 0.397 [m/s]. The deviation in the initial volume can partly be explained by the simplifed Rayleigh damping model. The deviation in entrapped air volume explains the larger natural period for the BEM. The free surface for the BEM at the same time instants as in figure 4 is seen in figure 6. The first image is just prior to the first pressure maximum. It is seen that the wetted length is larger for both BEM models compared to the experiments. The air water interaction is hence not properly modelled. During the compression of the air pocket an overestimation of the wetted length yields too large pressures, since more water must be accelerated. The period of time corresponding to the largest decay of the pressure time history corresponds to the time when the change in the wetted length of the roof is largest. Hence the change of the wetted length is suggested to play an important role in explaining the decay of the pressure signal. For the experiments the ratio between the first pressure maximum to the first pressure minimum is 0.58 while the corresponding numerical ratio is 0.70 for the undamped and 0.72 for the damped BEM model.

To view the air pocket as a simple mass-spring system seems to be questionable for accurate estimates. The system of the air pocket and the surrounding water does not obtain the same geometrical shape periodically. Hence there is no reason to expect the pressure to reproduce periodically either. It is believed that one of the reasons for the decay is that the air pocket energy is transfered to the liquid, i.e. we are not able to point out any significant energy dissipation source. Potential dissipation sources have been discussed by Faltinsen and Timokha [1]. From the experiments it is also seen that air leakage, if present, have a strong damping effect.

The present numerical model will be improved to more fully take into account the effect of air prior to closure. A compressible 1d model will be coupled with the BEM. The results of this investigation will be reported at the workshop.

References

[1] O. M. Faltinsen and A. N. Timokha. *Sloshing*. Cambridge University Press, 2009.

[2] S. Zhang, D. K. P. Yue, and K. Tanizawa. Simulation of plunging wave impact on a vertical wall. *Journal of Fluid Mechanics*, 327:221–254, 1996.

[3] M. Greco, M. Landrini, and O.M. Faltinsen. Local hydroelastic analysis of a VLFS with shallow draft. In *Hydroelasticity in Marine Technology, 2003 Oxford*, 2003.